Nonisotropic and nonsingle explosion in central ^{129}Xe + ^{120}Sn collisions at 50–125 MeV/nucleon

Jun Su,[1,2] Konstantin Cherevko,[1,2] Wen-Jie Xie,[1,2] and Feng-Shou Zhang[1,2,3,*]

[1]*Key Laboratory of Beam Technology and Material Modification of Ministry of Education, College of Nuclear Science and Technology, Beijing Normal University, Beijing 100875, China*

[2]*Beijing Radiation Center, Beijing 100875, China*

[3]*Center of Theoretical Nuclear Physics, National Laboratory of Heavy Ion Accelerator of Lanzhou, Lanzhou 730000, China*

(Received 9 June 2013; published 30 January 2014)

The expanding dynamics in central ^{129} Xe + ^{120}Sn collisions at 50 MeV/nucleon is investigated within the framework of the isospin-dependent quantum molecular dynamics model in combination with the statistical decay code GEMINI. The nonisotropic distributions in the fragment size and average kinetic energy are reproduced. The collective expansion energy and the Coulomb explosion energy of different fragments are extracted. We focus on the nonisotropic explosion of the colliding system and the difference of explosion energies of H, He, Li, and Be fragments. The radial flow energies are extracted at the polar angle $\theta_{c.m.} = 90^{\circ}$. From studying the beam energy dependence at 50–125 MeV/nucleon, the threshold energies of the radial flow are investigated. The time evolutions of the density and the collective velocity are investigated. It is found that the radial flow causes the system to expand in the isotropic direction, whereas the residual incident energy causes the system to extend along the longitudinal direction. The Pauli blocking is responsible for the nonisotropic nature of the collective velocity.

DOI: 10.1103/PhysRevC.89.014619 PACS number(s): 25.70.Pq, 25.75.Ld

I. INTRODUCTION

The studies of heavy-ion collisions (HICs) are motivated by purpose of extracting information on the nuclear equation of state far away from the saturation region [1]. Indeed, for this purpose one has to analyze the entire reaction dynamics in which the collective motion is supposed to play an important role [2–5]. The collective motion has been observed in HICs over a wide range of incident energies [6,7]. Particularly, the radial flow characterizes particles that are emitted from a source with a common velocity field independent of the direction. Experimental extraction of radial flow is based on the phenomena that the kinetic energy spectra of particles from identified single source, such as in central collisions, do not show the characteristic Boltzmann-like shape expected for thermal emission [8]. Assuming a form characterized by radial velocity parameters, the radial flow was extracted by fitting the measured energy spectra [9–11]. The radial flow was also deduced from the quasilinear dependence of the average kinetic energy on the mass of the emitted fragment [11–15]. The systematic data in central collisions show that the radial flow energies increase with the incident energy. An interest in measurement of radial flow at low incident energies centers on the interpretation of the threshold value for collective expansion [16,17]. For instance, the extra radial flow on ^{36}Ar + ^{27}Al collisions between 55 and 95 MeV/nucleon was found to gradually decrease to zero as the excitation energy reaches values between 5 and 6 MeV/nucleon [18]. Despite the difference in the methods of the determination, it can be concluded that radial flow beyond the Coulomb flow starts to be seen around 5 MeV/nucleon of the available energy [7,19].

In the simple thermodynamic fireball model, breakup of the hot equilibrated nuclear system results in a purely thermal energy spectra that is Maxwell-Boltzmann type in the classical limit [20,21]. In order to gain a quantitative understanding of the spectra, Siemens and Rasmussen develop this model by introducing the blast-wave picture, in which the isotropic hydrodynamical expansion is considered to be responsible for the deviation from the purely thermal distribution of the energy spectra [9]. A qualitative analysis of the spherical expansion was given within the framework of relativistic hydrodynamics, in which linear relation between the flow velocity and the position vector was found [22]. Actually, the linear relation $\beta_f = \mathrm{Hr}$ was used in the earlier work by Bondorf *et al.* studying the isotropic self-similar expansion of an ideal gas into vacuum [23]. The basic concept of the self-similar expansion was applied to analyze the experimental data both by the ALADIN Collaboration and FOPI Collaboration [13,24,25]. However, it was found that isotropic self-similar flow parametrizations were not sufficient for the adequate description of the kinetic energies within the metropolis multifragmentation Monte Carlo model for nonspherical sources (MMMC-NS) [26].

Transport models are used to investigate the origin of the radial flow. Based on the framework of the quantum molecular dynamics (QMD) model, Hartnack and Aichelin found that there are three dynamical contributions to the collective effect, including initial- and final-state correlations, potential interactions, and collisions [27]. However, the compression phase followed by a larger collective flow was observed in central collisions at 50 MeV/nucleon within the framework of the stochastic mean-field approach [28]. The isospin dependence of radial flow was investigated based on the transport model [29,30,32]. Within the framework of the isospin-dependent quantum molecular dynamics (IQMD) model, the strong isospin dependence of the radial flow from the symmetric central collisions at incident energies of a few hundred MeV/nucleon is shown [29–31]. However, it is found

*Corresponding author: fszhang@bnu.edu.cn

that the effect of symmetry energy on radial flow is weak within the isospin-dependent Boltzmann-Uehling-Uhlenbeck (BUU) model [32]. The linear relation between the radial flow velocity and the position vector is found both in isospin-dependent BUU model [32] and the framework of the stochastic transport theory [33]. The microcanonical lattice gas model was applied to test the effect of radial flow on fragment formation. It is found that the disordered thermal motion is always more efficient than the collective motion to break up the system [34,35].

Based on the amount of available data of radial flow, some complications emerge, especially at low energy. First, the spherical symmetry of velocity space topology even for very central events has to be inspected [36]. It has been found that the Pauli blocking is responsible for the nonequilibrium in central HICs around Fermi energy [37]. Thus, in order to extract information of the fermionic feature in HICs, studies of the deviations from sphericity of radial flow are of increasing importance as the energy and the system size are lowered [7,38]. Second, the concept of a single flow velocity provides a useful way to parametrize the data, but it is quite simplistic. The experimental data suggested that all fragments do not participate equally in the collective expansion. Hsi *et al*. found that the values for collective expansion energies, extracted independently for each charge fragment in central Au + Au collisions at 100 MeV/nucleon, decrease with the fragment charge [10]. Another evidence is that the kinetic energy rises with fragment size only for relatively light fragments, but then tends to decrease again for heavier fragments [39]. Third, the Coulomb expansion dynamics and the radial flow have a similar influence on the kinetic energy. The Coulomb energy becomes an important background to the radial flow at low incident energy [10,14]. The systematic data for radial flow energy show values similar to the estimate of radial energy for a pure Coulomb explosion when the incident energy is about 50 MeV/nucleon [7,19]. Fourth, some scalings of the radial flow, which indicates that the radial expansion plays an important role on the fragment formation, was found. The amount of radial collective energy fixes the mean fragment multiplicity for a given total excitation energy [4,5]. The radial flow was also found to be correlated to the global stopping in central collisions [37,40,41].

In order to understand those complications and the puzzling aspects, the collective expansion in central HICs at 50–125 MeV/nucleon is investigated within the framework of the IQMD model in combination with the statistical decay code GEMINI. The experimental data for central reaction ^{129}Xe + ^{120}Sn are relatively abundant. Comparison between the calculation and the experimental data can improve the credibility of the model. Thus, the reactions ^{129}Xe + ^{120}Sn are chosen in this work. This paper is organized as follows. In Sec. II, the theoretical model is introduced briefly. In Sec. III, the results are presented. The collective expansion energies and the Coulomb explosion energies of different fragments are extracted and compared in the assumption of spherical expansion in Sec. III A. Based on the reproduction of angular anisotropy in the distributions of fragment yield and kinetic energy, the angular distributions of the collective expansion energies and the Coulomb explosion energies are investigated in Sec. III B. Then in Sec. III C, the topology of collective velocity field and nucleonic density is studied. The collective velocities as a function of the radial distances both at forward angles and sideward angles are shown. Finally, the conclusion is given in Sec. IV.

II. THEORETICAL FRAMEWORK

In this work, the IQMD model [42,43] is applied to describe the formation of the pre-fragments. In order to compare the calculations with the experimental data, the GEMINI model [44] is applied to simulate the decays of the prefragments.

A. Isospin-dependent quantum molecular dynamics model

The wave function for each nucleon in the IQMD model is represented by a Gaussian wave packet

$$\phi_i(\mathbf{r},t) = \frac{1}{(2\pi L)^{3/4}} e^{-\frac{[\mathbf{r}-\mathbf{r}_i(t)]^2}{4L}} \cdot e^{\frac{i\mathbf{r}\cdot\mathbf{p}_i(t)}{\hbar}}, \tag{1}$$

where $\mathbf{r}_i$ and $\mathbf{p}_i$ are the average values of the position and momentum of the ith nucleon, and L is related to the extension of the wave packet. The total N-body wave function is assumed to be the direct product of these coherent states. Through a Wigner transformation of the wave function, the N-body phase-space distribution function is given by

$$f(\mathbf{r},\mathbf{p},t) = \sum_{i=1}^{N} \frac{1}{(\pi\hbar)^3} e^{-\frac{[\mathbf{r}-\mathbf{r}_i(t)]^2}{2L}} e^{-\frac{[\mathbf{p}-\mathbf{p}_i(t)]^2\cdot 2L}{\hbar^2}}. \tag{2}$$

The time evolutions of the nucleons in the system under the self-consistently generated mean-field are governed by Hamiltonian equations of motion

$$\dot{\mathbf{r}}_i = \nabla_{\mathbf{p}_i} H, \quad \dot{\mathbf{p}}_i = -\nabla_{\mathbf{r}_i} H, \tag{3}$$

where the Hamiltonian H is expressed as

$$H = T + U_{\mathrm{Coul}} + \int V_{\mathrm{nucl}}[\rho(\mathbf{r})]d\mathbf{r}. \tag{4}$$

Here, the first term T is the kinetic energy, the second term U_{Coul} is the Coulomb potential energy, and the third term is the nuclear potential energy. Each term of the nuclear potential energy-density functional V_{nucl} reads

$$V_{\mathrm{nucl}} = V_{\mathrm{Sky}} + V_{\mathrm{sur}} + V_{\mathrm{sym}}, \quad V_{\mathrm{Sky}} = \frac{\alpha}{2}\frac{\rho^2}{\rho_0} + \frac{\beta}{\gamma+1}\frac{\rho^{\gamma+1}}{\rho_0^{\gamma}},$$
$$V_{\mathrm{sur}} = \frac{g_{\mathrm{sur}}}{2}\frac{(\nabla\rho)^2}{\rho_0}, \quad V_{\mathrm{sym}} = \frac{C}{2}\frac{(\rho_n-\rho_p)^2}{\rho_0}. \tag{5}$$

Here, ρ is the density, and ρ_0 is the saturation density. V_{Sky} describes the saturation properties and compressibility of nuclear matter. The soft equations of state with a compressibility of 200 MeV at saturation density is applied in the present work. V_{sur} is the surface term to describe the surface property of finite nuclei. V_{sym} is the symmetry term, which is crucial for reproducing the isospin-dependent effect in the dynamics. The parameters of the nuclear potential energy adopted in the present work are shown in Table I.

The binary nucleon-nucleon (NN) collisions are included in the IQMD model. The NN collisions mimic the effect of

TABLE I. The parameters of the nuclear potential energy adopted in the present work.

α (MeV)	β (MeV)	γ	g_{sur} (MeV $\cdot$fm^5)	C (MeV)	ρ_0 (fm^{-3})	K (MeV)	E_0/A (MeV)
−356	303	7/6	130	39.4	0.16	200	−16.1

the short-range repulsive residual interaction together with the stochastic change of the phase space distribution. The differential cross sections of NN collisions can be written as

$$\left(\frac{d\sigma}{d\Omega}\right)_{\text{el(inel)}} = \sigma^{\text{free}}_{\text{el(inel)}} f^{\text{angl}}_{\text{el(inel)}} f^{\text{med}}_{\text{el(inel)}}, \quad (6)$$

where σ^{free} is the cross section of NN collisions in free space and f^{angl} gives the angular distribution. The isospin-dependent parametrization of σ^{free} and f^{angl} adopted in this work are taken from Ref. [45]. f^{med} gives the in-medium corrections to the NN cross section. The in-medium factor of $f^{\text{med}} = 1 - 0.2\rho/\rho_0$ [46] is adopted.

To compensate for the fermionic feature the method of the phase space density constraint in the CoMD model [47] is applied. The phase space occupation probability $\overline{f}_i$ is calculated by performing the integration on an hypercube of volume h^3 in the phase space centered around the ith nucleon at each time step.

$$\overline{f}_i = \sum_n \delta_{\tau_n,\tau_i}\delta_{s_n,s_i}\int_{h^3}\frac{1}{\pi^3\hbar^3}e^{-\frac{(\mathbf{r}_n-\mathbf{r}_i)^2}{2L}-\frac{(\mathbf{p}_n-\mathbf{p}_i)^2 L}{\hbar^2}}d^3r d^3p. \quad (7)$$

Here, τ_i represents isospin degree of freedom. s_i is the spin projection quantum number of the ith nucleon. At each time step and for each nucleon, the phase space occupation $\overline{f}_i$ is checked. If phase space occupation $\overline{f}_i$ has a value greater than 1, the momenta of the ith nucleon is changed randomly by many-body elastic scattering.

In addition, Pauli blocking, which is related to the phase space density constraint, is taken into account. Whenever a collision occurs, the phase space occupation $\overline{f}_i$ is calculated. Only if such functions at the final states are both less than 1 is the scattering accepted.

In the present work, the simulation time by IQMD is up to 500 fm/c. At the end of the IQMD evolutions, a phase-space coalescence method [42,48] is applied to formate the prefragments. In this coalescence method, nucleons with relative distance of coordinate and momentum of $|\mathbf{r}_i - \mathbf{r}_j| \leq R_0$ and $|\mathbf{p}_i - \mathbf{p}_j| \leq P_0$ belong to a cluster. Here, R_0 and P_0 are phenomenological parameters determined by fitting the global experimental data, such as the multiplicities. Values of R_0 and P_0 used in this work are 3.2 fm and 250 MeV/c. In order to get rid of the nonphysical clusters, two conditions need to be satisfied. First, it is checked whether the cluster is an isotope existing in the nuclear data sheets, and if it is, then the cluster can be accepted. Second, the condition of $R_{\text{rms}} < 1.14A^{1/3}$ is used to get rid of the nonphysical line-type clusters. Here, the R_{rms} and A are the root-mean-square radius and mass number of the cluster, respectively. Finally the mass numbers, charge numbers, and excitation energies of the accepted clusters (prefragments) are calculated and used as the inputs in GEMINI model.

B. GEMINI

The statistical model GEMINI is widely used in performing sequential decays of hot fragments. It allows not just light-particle evaporation and symmetric fission but all possible binary-decay modes. A Monte Carlo technique is employed to follow all decay chains until the resulting products are unable to undergo further decay. The partial decay widths are taken from the Hauser-Feshbach formalism for light-particle evaporation, and from Moretto's generalized transition-state formalism for more symmetry divisions. Nuclear masses with shell and pairing corrections are adopted. Nuclear level densities were taken as a Fermi-gas form. The details of GEMINI are given in Ref. [44].

III. RESULTS AND DISCUSSION

Via the IQMD model accompanied by the GEMINI model, the study of multifragmentation in central HICs at intermediate energies have been presented in the previous work [49]. The multiplicities and the kinetic energy spectra have been calculated and compared with the experimental data. A good agreement has been observed. This work focuses on the kinetic characteristics and collective expansion.

A. Average kinetic energy and expansion

One of the experimental evidences for the existence of radial expansion is the quasilinear dependence of the average kinetic energy on the mass or charge of the emitted fragment. The average kinetic energy in central ^{129}Xe + ^{120}Sn collisions has been measured by the INDRA Collaboration [26,50,51]. Figure 1 shows the comparison between the experimental data

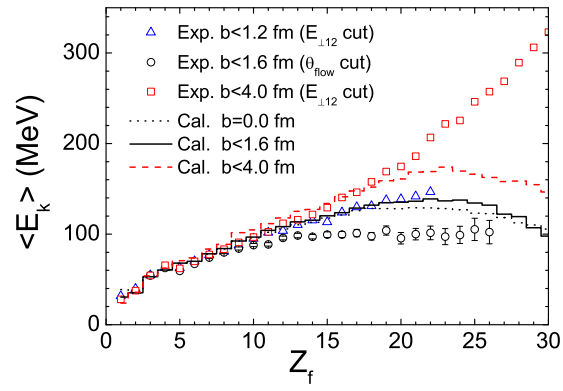

FIG. 1. (Color online) Average kinetic energy in the center of mass as a function charge in central ^{129}Xe + ^{120}Sn collisions at 50 MeV/nucleon. The experimental data for central events are selected using transverse energy of light charged particles $E_{\perp 12}$ [26,50] and flow angle θ_{flow} [51].

and calculations of the average kinetic energies in the center of mass as a function of fragment charge in central ^{129}Xe + ^{120}Sn collisions at 50 MeV/nucleon. Experimentally, the transverse energy of light charged particles $E_{\perp 12}$ and flow angle $\theta_{\rm flow}$ are used to select the central events. In the region of $Z_f < 10$, the experimental kinetic energy rises quasilinearly with the fragment charge and is independent on experimental event selections. When the fragment charge is larger than 10, the differences between the event selections emerge. For the $\theta_{\rm flow}$ selection, the average kinetic energies for each Z_f is almost the same in the region of $Z_f > 10$. For the $E_{\perp 12}$ selection, the average kinetic energy increases with the Z. It is shown that from experimental data for the same selection (triangles and squares), the kinetic energy of the fragment with $Z_f > 15$ is rather dependent on the impact parameter.

Theoretically, the central ^{129}Xe + ^{120}Sn collisions at 50 MeV/nucleon with impact parameters of $b = 0$ fm, $b < 1.6$ fm, and $b < 4.0$ fm are simulated respectively by the IQMD + GEMINI model. The calculated average kinetic energy is shown in Fig. 1. The calculations reproduce the quasilinear increase of the experimental data in the region of $Z_f < 10$. The differences of the overall trends between the calculations and experimental data are shown for the large fragments. The calculated average kinetic energy increases, then saturates and decreases for $Z_f > 20$. The average kinetic energies of the large fragments are sensitive to the methods to select the central events. Thus, differences of the methods to select the central events are responsible for the differences of the overall trends in the region of $Z_f > 10$. By comparing calculations with different impact parameters, it is found that the calculated average kinetic energy is almost independent of the impact parameters in the region of $Z_f < 10$. However, the calculated average kinetic energy of fragments with $Z_f > 10$ increases with the impact parameter.

For the central HICs, the average kinetic energy $\langle E_k \rangle$ of fragments can be written as

$$\langle E_k \rangle = E_{\rm ran} + E_{\rm rad}. \tag{8}$$

Here, $E_{\rm ran}$ reflects the kinetic energy of random motions, which includes the thermal motion and Fermi motion. $E_{\rm rad}$ is the radial expansion energy. In the assumption of Fermi-Dirac distribution and the case of finite temperature, the random kinetic energy can be written as [8]

$$E_{\rm ran} = \frac{\int d\epsilon \frac{\epsilon^{3/2}}{1+\exp(\frac{\epsilon-\mu}{T})}}{\int d\epsilon \frac{\epsilon^{1/2}}{1+\exp(\frac{\epsilon-\mu}{T})}}, \tag{9}$$

where μ is the chemical potential and T is thermal temperature. The radial expansion of the fragments in central collisions is a combination of the collective expansion and the Coulomb expansion. The radial expansion energy $E_{\rm rad}$ can be nonrelativistically approximated by [10]

$$\begin{aligned} E_{\rm rad} &= E_{\rm coll} + E_{\rm Coul} \\ &= \frac{3}{5}\left[\frac{1}{2}A_f m_0 c^2 \beta_{\rm coll}^2 + \frac{Z_f(Z_s - Z_f)e^2}{R_s}\right], \end{aligned} \tag{10}$$

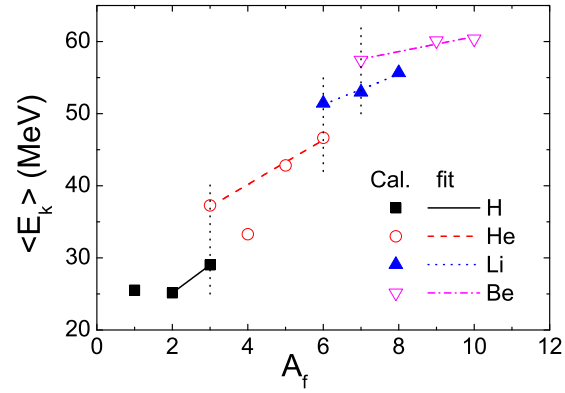

FIG. 2. (Color online) Average kinetic energy in the center-of-mass as a function mass in central ^{129}Xe + ^{120}Sn collisions at 50 MeV/nucleon by IQMD + GEMINI model. The linear fits of average kinetic energy for isotopes respectively are also shown.

where A_f and Z_f are the mass number and charge number of the fragment and Z_s and R_s are the charge number and radius of the fragmenting source.

As the random kinetic energy $E_{\rm ran}$ and the Coulomb expansion energy $E_{\rm Coul}$ is independent of mass number A_f, the collective expansion energy $E_{\rm coll}$ can be extracted by the linear fit of the relationships between the average kinetic energy and mass number A_f for the isotopes. Figure 2 shows the average kinetic energies of H, He, Li, and Be isotopes as functions of mass number. The linear fits of average kinetic energy for H, He, Li, and Be isotopes respectively are also shown. Except for proton and α particles, the average kinetic energy increases with the mass number of the fragments. Since the protons and α particles are exclusively produced by the secondary decays of the prefragments, the kinetic energies of them not only reflect the kinetic properties of fragmenting source but also carry the kinetic information of the decay steps of the prefragments. Due to this possible complexity, the kinetic energies of proton and α particles are not considered for linear fits. One can also see that the points for proton and α particles in Fig. 2 keep away from the fitted lines.

It can be seen from Eqs. (9) and (10) that the random kinetic energy $E_{\rm ran}$ and the collective expansion energy $E_{\rm coll}$ is independent of charge number Z_f. In central ^{129}Xe + ^{120}Sn collisions at 50 MeV/nucleon, and the charge number of the fragmenting source Z_s is much larger than the charge numbers of He, Li, and Be. For this reason, the Coulomb expansion energy per charge can be extracted by the difference of average kinetic energy between isobars. In Fig. 2, there are three isobar pairs (^{3}H-^{3}He, ^{6}He-^{6}Li, and ^{7}Li-^{7}Be). The vertical dotted lines are for guiding those isobar pairs. One can see that the average kinetic energies for isobars are different. The average kinetic energies for isobars with large Z_f are larger than those in the small charge cases. Those differences are the consequence of the Coulomb expansion.

The above method to extract the collective expansion energy and the Coulomb expansion energy is applied to the central ^{129}Xe + ^{120}Sn collisions at 50 MeV/nucleon with impact parameters of $b = 0$ fm, $b < 1.6$ fm, and

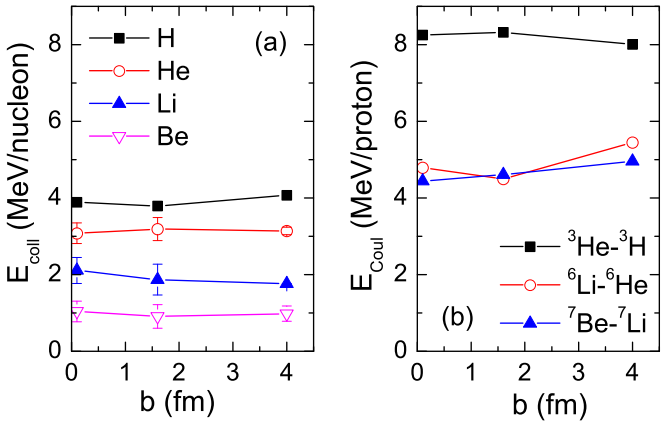

FIG. 3. (Color online) Collective expansion energy per nucleon and Coulomb expansion energy per charge as a function of impact parameter. The error bars come from the fits of the kinetic energies.

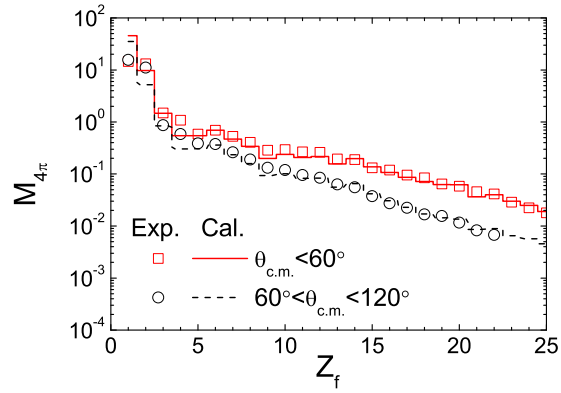

FIG. 4. (Color online) Average multiplicity of fragments as a function of charge in central ^{129}Xe + ^{120}Sn collisions at 50 MeV/nucleon. Squares and solid line represent the results for forward angles ($\theta_{c.m.} < 60^\circ$), and circles and dashed lines represent results for sideward angles ($60^\circ < \theta_{c.m.} < 120^\circ$). Experimental data are taken from Refs. [26].

$b < 4.0$ fm. The results are shown in Fig. 3. In fact, the average kinetic energies of fragments emitting from any angle are all included. In other words, the assumption of isotropic expansion is implied. It can be seen from Fig. 3(a) that the collective expansion energy per nucleon is almost independent of the impact parameter in the region of $b < 4.0$ fm. The collective expansion energies per nucleon for H, He, Li, and Be are different. It means that all fragments do not participate equally in the collective expansion. The collective expansion energy per nucleon decreases with the increasing charge number of fragments. For the collisions with $b < 1.6$ fm, the collective expansion energies per nucleon for H, He, Li, and Be fragments are 3.8, 3.2, 1.9, and 0.91 MeV/nucleon. The gradually decreasing trend of the collective expansion energy with the fragment charge strongly supports the result proposed by Hsi *et al*. [10].

As shown in Fig. 3(b), the Coulomb expansion energy E_{Coul} in MeV/proton is also independent of the impact parameter for each isobars. From the approximated formula [Eq. (10)], it can be seen that the Coulomb expansion energy in MeV/proton is $(Z_s - Z_f)e^2/R_s$. For fragments with $Z_f \ll Z_s$, the values of Coulomb expansion energy in MeV/proton should be similar. The values of E_{Coul} extracted from the isobar pairs of ^{6}He-^{6}Li and ^{7}Li-^{7}Be are both around 5 MeV/proton. However, the value of E_{Coul} extracted from the isobar-pairs of ^{3}H-^{3}He is about 8 MeV/proton, which is larger than the values extracted from the isobar pairs of ^{6}He-^{6}Li and ^{7}Li-^{7}Be. By comparing the Coulomb expansion energy with the the collective expansion energy, it can be found that the former is larger than the latter. This supports the inference that the Coulomb energy becomes an important background to the collective flow at low incident energy [10,14].

B. Angular distributions of the expansion energies

In the above investigation, the assumption of isotropic expansion is implied. In fact, the expansion of the fragmenting source is angular dependent. The angular isotropy in the distributions of fragment yield and fragment kinetic energy have been found from the INDRA experimental data [26].

Figure 4 shows the average multiplicity of fragments as a function of charge emitting from the forward region ($\theta_{c.m.} < 60^\circ$) and sideward region ($60^\circ < \theta_{c.m.} < 120^\circ$) in central ^{129}Xe + ^{120}Sn collisions at 50 MeV/nucleon. For the experimental data, it can be seen that the fragments with same charge are produced more abundantly in the forward region than in the sideward region. The difference between forward multiplicity and sideward multiplicity increases with increasing charge. The multiplicities in forward and sideward for $Z \leq 2$ are similar. This has been regarded as the autocorrelation produced by the $E_{\perp 12}$ selection method. The calculations by IQMD + GEMINI model show the enhancement in the forward region for all fragments. The agreement between the calculations and the experimental data is quite encouraging.

Figure 5 shows the average kinetic energy in the center-of-mass of fragments as a function of charge emitting from the forward and sideward angular regions in central ^{129}Xe + ^{120}Sn collisions at 50 MeV/nucleon. The anisotropy of the kinetic energy is shown obviously. For the same fragment, the average kinetic energy of the forward case is larger than that of the sideward case. The anisotropy of the kinetic energy becomes more apparent when the fragment charge increase. The calculations generally agree with the experimental data. An acceptable divergence appears for the sideward case for $Z > 10$. As mentioned above, the differences of the methods to select the central events are responsible for this differences. In addition, due to the phenomenological method to compensate for the fermionic feature used in the model, there are some differences of the incomplete stopping between the experimental data and model calculations [37]. This is another physical reason responsible for the divergence appears for the sideward case for $Z > 10$. The good agreement of the nonisotropic multiplicity and kinetic energy between the calculations and the data suggests that the IQMD + GEMINI model is robust and reasonable to investigate the anisotropy of the expansion in central HICs. Actually, the incomplete

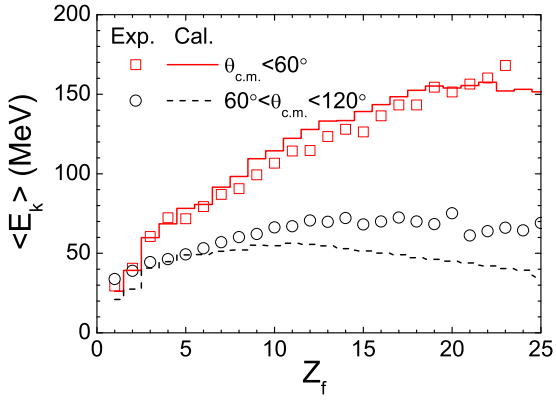

FIG. 5. (Color online) Average kinetic energy in the center of mass as a function charge in central ^{129}Xe + ^{120}Sn collisions at 50 MeV/nucleon. Squares and solid line represent the results for forward angles ($\theta_{c.m.} < 60°$), and circles and dashed lines represent results for sideward angles ($60° < \theta_{c.m.} < 120°$). Experimental data are taken from Ref. [26].

stopping, which indicates the nonequilibrium and residual memory, has been reproduced by the IQMD + GEMINI model in our previous work [37].

The anisotropy of the expansion is demonstrated by the polar-angle-dependent collective expansion energy $E_{\rm coll}$ and Coulomb expansion energy $E_{\rm Coul}$. The collective expansion energies per nucleon as a function of polar angle in central ^{129}Xe + ^{120}Sn collisions at 50 MeV/nucleon with $b = 0$ fm are shown in Fig. 6. The collective expansion energies $E_{\rm coll}$ are extracted by the linear fits of the relationships between the average kinetic energy and mass number A_f. The error bars of the collective expansion energy come from linear fits of the kinetic energies. For central ^{129}Xe + ^{120}Sn collision, the masses of the projectile and target are almost the same. The plane symmetry of the dynamical evolution in the center of mass will hold. Thus, the values of the collective expansion energy $E_{\rm coll}$ and Coulomb expansion energy $E_{\rm Coul}$ at the polar angle θ and $\pi - \theta$ are extracted simultaneously. One can see that the longitudinal value of $E_{\rm coll}$ is larger than the transversal one for all considered fragments. From $\theta_{c.m.} = 0°$ to 90°, the values of $E_{\rm coll}$ decrease monotonously. Expressly for Be fragment [Fig. 6(d)], the value of $E_{\rm coll}$ at $\theta_{c.m.} = 0°$ is 5 MeV/nucleon, which is much larger than the values at other emitting angle.

The collective expansion energy at $\theta_{c.m.} = 90°$ is the radial flow energy. From this perspective the radial flow energies of H, He, Li, and Be fragments are 2.0, 0.8, 0.9, and 0.4 MeV/nucleon respectively. Only the radial flow energy of H fragment is close to the value of 2.2 MeV/nucleon extracted by Statistical Multifragmentation Model [3], in which the concept of a single flow velocity is adopted. The radial flow energy of Be fragment is close to zero within a margin of error.

The radial flow energies of H, He, Li, and Be fragments are extracted in central ^{129}Xe + ^{120}Sn collisions at incident energy between 50 to 125 MeV/nucleon. The results are shown in Fig. 7. It can be seen from the figure that the calculated results show the mass dependence of radial flow. The increasing trend of the radial flow energy with fragment charge is found at each incident energy except 50 MeV/nucleon. From studying the beam energy dependence, it could be found that the radial flow energy in the reaction disappears at an incident energy, which is called the threshold energy of radial flow. The lines in Fig. 7 are the linear fits of the calculated results. It is shown that the radial flow energies increase as the incident energies increase, and the linear relations between the radial flow energy and incident energy are quite satisfied. From the fitting lines, the values of threshold energies for H, He, Li, and Be fragments are 24.9, 34.7, 34.8, and 42.0 MeV/nucleon respectively. The threshold energies of radial flow increase with the increasing

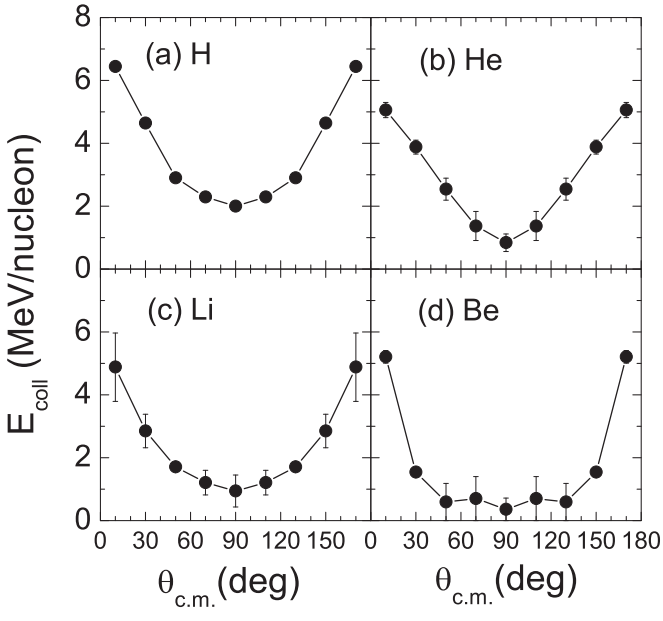

FIG. 6. Collective expansion energy per nucleon as a function of polar angle in central ^{129}Xe + ^{120}Sn collisions at 50 MeV/nucleon with $b = 0$ fm. The error bars come from the fits of the kinetic energies.

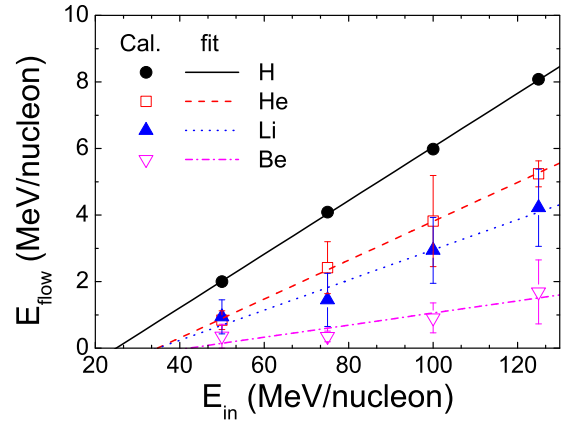

FIG. 7. (Color online) Radial flow energies of H, He, Li, and Be fragments in central ^{129}Xe + ^{120}Sn collisions at incident energy between 50 to 125 MeV/nucleon.

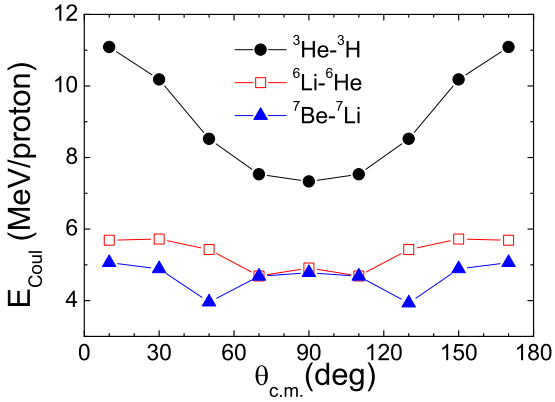

FIG. 8. (Color online) Coulomb expansion energy in MeV/proton as a function of polar angle in central ^{129}Xe + ^{120}Sn collisions at 50 MeV/nucleon with $b = 0$ fm.

fragment charge. Only the threshold energy of the radial flow extracted by Be fragment is close to the value in Ref. [31], in which the concept of a single flow velocity is adopted.

Figure 8 shows the Coulomb expansion energy in MeV/proton as a function of polar angle. It can be seen from the figure that the values of E_{Coul} extracted from the isobar-pairs of ^{6}He-^{6}Li and ^{7}Li-^{7}Be are 5 MeV/proton in any angle. The polar angle dependence is indefinable. However, the Coulomb expansion energy extracted from isobar-pair of ^{3}H-^{3}He shows the obvious polar angle dependence. From $\theta_{c.m.} = 0^{\circ}$ to 90°, the value of E_{Coul} decreases from 11 to 8 MeV/proton. Comparing the value of E_{Coul} with the radial flow energy, it can be seen that the Coulomb expansion dominates in the fragmenting source.

C. Topology of collective velocity field

In order to reveal the dynamic processes which are responsible for the nonisotropic distribution of the fragment size, kinetic energy, and expansion energy, the topology of collective velocity field is investigated. Figures 9 and 10 display the time evolutions of the density and the collective velocity in the x-z plane and x-y plane respectively. Here, x is the direction of the impact parameter, and z is the beam direction. The density is shown as colors. The collective velocity in each specific spatial position is calculated within 10 000 events and shown as arrows.

As shown in Fig. 9, the dynamic process in x-z plane is characterized as flowing. At $t = 0$ fm/c, the projectile and target move close to each other. The collective velocity of the nucleons is the same as the incident velocity. At $t = 10$ fm/c, the projectile and target contact with each other. Due to the exchange of the nucleons, the density of the contact area increases to about 0.4 ρ_0. The collective velocity of the peripheral nucleons is not directed along the z axis strictly. At $t = 30$ fm/c, part of two nuclei overlap. The density of central region reach to 1.2 ρ_0. The nucleons outside the overlap region are slowing down but still move to the center. The collective velocity in the overlap region deviates obviously from the incident direction and has a large part of transverse component. In the overlap region, a large number of nucleon-nucleon collisions occur. Consequently the incident energy transfers both to the thermal kinetic energy and the collective energy along the transverse direction. The Pauli principle is responsible for the transverse energy transfer. Some nucleons are squeezed out at the sideward angles.

At $t = 50$ fm/c, the projectile and target overlap completely. The transverse momentum causes the overlap region to expand radially and thus the density of central region decreases to ρ_0. The distribution of the density is isotropic. The nucleons are squeezed out along the sideward direction. The collective velocity in the peripheral region is directed along the x axis approximatively, while that in the central region shows as zero. Nevertheless, this does not mean that the incident energy dissipate completely. It has been found that a part of the incident energy remains in central HICs at Fermi energy [37]. The residual incident momentums of the projectile and the target have a opposite direction, thus the

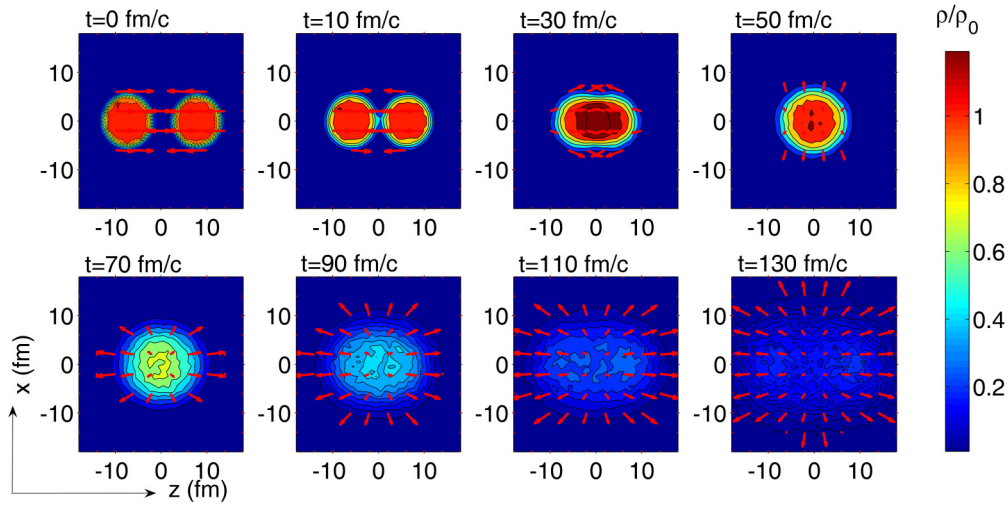

FIG. 9. (Color online) Time evolutions of the density (colors) and the collective velocity (arrows) in the x-z plane in central ^{129}Xe + ^{120}Sn collisions at 50 MeV/nucleon with $b = 0$ fm.

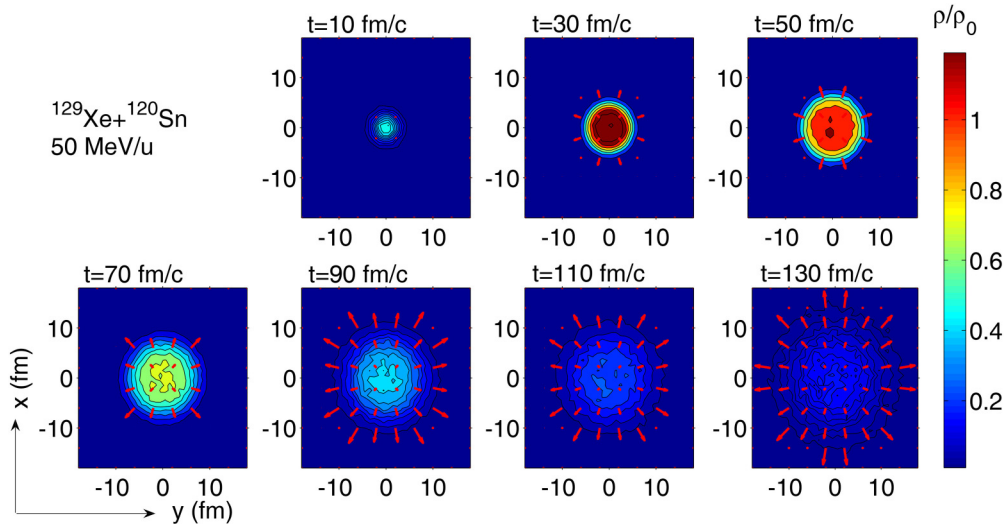

FIG. 10. (Color online) Same as Fig. 9 but in the x-y plane.

collective velocity in the overlap region gets close to zero. At $t = 70$ fm/c, the density of central region decreases to about 0.7 ρ_0. The distribution of the density is also isotropic. The collective velocities at forward angles are larger than those at sideward angles. That is to say, the residual incident momentums emerge at $t = 70$ fm/c, while they are covered up in distribution of the collective velocity at $t = 50$ fm/c. It is supposed that the Pauli blocking is responsible for the residual incident energy and the nonisotropic nature of the collective velocity. In central HICs near Fermi energy, most of the binary collisions are blocked. Therefore, most of the particles maintain their incident energy and consequently the colliding system becomes more transparent.

At $t = 90$ fm/c, the density of central region decrease to about 0.5 ρ_0. The distribution of the density has an elliptic form. The system extend faster along the longitudinal direction. The collective velocity is nonisotropic and dependent on the distance. The collective velocity in the peripheral region is larger obviously than that in the cental region. At $t = 110$ fm/c, the system continue to expand nonisotropically. The density of central region decreases to 0.3 ρ_0. At $t = 130$ fm/c, the density of central region reaches 0.2 ρ_0, which is lower limit of the freeze-out density [19]. Therefore, the Coulomb expansion dominates after this time.

As shown in Fig. 10, the dynamic process in the x-y plane is characterized as flowing. At $t = 10$ fm/c, the projectile and target start to contact with each other. The region where the nucleons can be observed is very small. The density of central region is about 0.4 ρ_0. At $t = 30$ fm/c, many nucleons can be observed in the x-y plane. The nucleons in the central region are compressed. The density of central region reaches to 1.2 ρ_0. The collective velocity displays an outgoing radiational type. At $t = 50$ fm/c, the expansion process has started. The density of central region decreases to ρ_0. The distributions of the density and collective velocity are both isotropic. At $t = 70$ fm/c, the density of central region decreases to about 0.7 ρ_0. The collective velocity increases compared with that at $t = 50$ fm/c. At $t = 90$, 110, and 130 fm/c, the density of central region decreases with the increasing time. The distributions of the density and collective velocity are all isotropic.

As can be seen from the above description, some features of the dynamic evolution in central ^{129}Xe + ^{120}Sn collisions at 50 MeV/nucleon can be seen. First, the compression phase occurs in about 20 fm/c after the projectile and target start to contact with each other. The density of central region reaches about 1.2 ρ_0. Second, the longitudinal expansion is faster than the transversal expansion. The configuration of the system in coordinate space becomes prolate type at 90 fm/c after the collision. The residual incident energy is considered to be responsible for the nonisotropic expansion. Third, the collective velocity is associated with the position vector in the expansion phase. The collective velocity in the peripheral region is larger obviously than that in the cental region.

Figure 11 shows the longitudinal and transverse collective velocity as a function of radius at $t = 90$, 110, and 130 fm/c. At those three moments, the central densities of the system are 0.54, 0.31, and 0.23 ρ_0 respectively, which

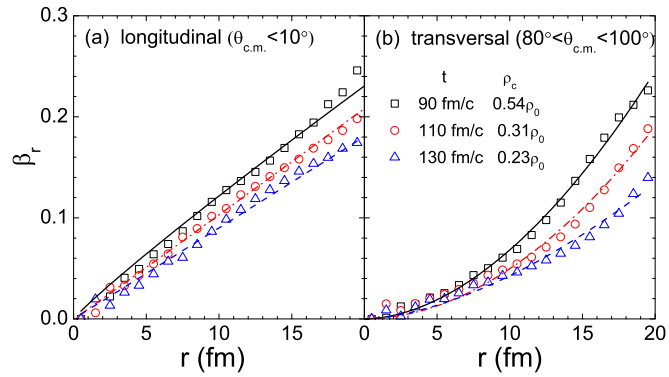

FIG. 11. (Color online) Longitudinal and transverse collective velocity as a function of radius at $t = 90$, 110, and 130 fm/c in central ^{129}Xe + ^{120}Sn collisions at 50 MeV/nucleon with $b = 0$ fm.

TABLE II. Fitting parameters of the relation $\beta_r = \beta_0 r^\alpha$ at 90, 110, and 130 fm/c in central ^{129}Xe + ^{120}Sn collisions at 50 MeV/nucleon with $b = 0$ fm.

t (fm/c)	ρ_c/ρ_0	α	
		$\theta_{c.m.} < 10^\circ$	$80^\circ < \theta_{c.m.} < 100^\circ$
90	0.54	0.92	1.84
110	0.31	1.11	1.94
130	0.23	1.00	1.65

are in the recognized region of the freeze-out density [19]. It can be seen from the figure that the collective velocity in the center is almost zero. The collective velocity increases with the increasing radius. Longitudinally, the increasing trend of the collective velocity is linear [Fig. 11(a)]. However, along the transverse direction the increasing trend is nonlinear [Fig. 11(b)]. Overall, the collective velocity along the longitudinal direction is larger then that along the transverse direction. The longitudinal collective velocity is almost twice as large as the transverse collective velocity for $r = 10$ fm.

The picture of self-similar expansion, in which the proportional relation $\beta_r = \beta_0 r$ holds, is widely adopted to analyze the experimental data by both the ALADIN Collaboration and FOPI Collaboration [13,24,25]. However, the relation $\beta_r = \beta_0 r^\alpha$ with $\alpha > 1$ is required when fitting the experimental data in the MMMC-NS model [26]. The collective velocity as a function of radius calculated by the IQMD + GEMINI model is fitted by the relation $\beta_r = \beta_0 r^\alpha$, as shown in Fig. 11. The fitting parameters is displayed in Table II. It can be seen that the time dependence of α is very weak for both the longitudinal direction and transverse direction. In the range of 90 to 130 fm/c, the expansion profile does not change, and the freeze-out configuration is accepted. For the longitudinal direction, the values of α are almost 1. The values of α for transverse direction are larger than 1. This is the reason why we draw a conclusion that the expansion profile is nonisotropic. The longitudinal expansion profile can be considered as self-similar expansion. However, the transverse expansion profile is a non-self-similar expansion with $\alpha > 1$. As shown in Figs. 9 and 10, the radial flow causes the system to expand isotropically, whereas the residual incident energy cause the system to extend along the longitudinal direction. Thus the residual incident energy is considered to be responsible for the nonisotropic expansion.

IV. CONCLUSION

In conclusion, the expanding dynamics in central ^{129}Xe + ^{120}Sn collisions at 50–125 MeV/nucleon is investigated within the framework of IQMD + GEMINI model. The nonisotropic distributions in the fragment size and average kinetic energy are reproduced. Based on the good agreements between the calculated kinetic energy and the experimental data, the collective expansion energy $E_{\rm coll}$ and the Coulomb explosion energy $E_{\rm Coul}$ of different fragments are extracted. It is found that the nonsingle flow is shown in the fragmenting source. The value of $E_{\rm coll}$ increases with the increasing fragment charge. The collective expansion and the Coulomb explosion coexist.

The anisotropy of the expansion is demonstrated by the polar angle $\theta_{c.m.}$ dependent collective expansion energy $E_{\rm coll}$ and Coulomb expansion energy $E_{\rm Coul}$. The value of $E_{\rm coll}$ reduces rapidly from $\theta_{c.m.} = 0^\circ$ to 90°. The radial flow energies, which are the collective expansion energies per nucleon at $\theta_{c.m.} = 90^\circ$, of H, He, Li, and Be fragments, in this work are 2.0, 0.8, 0.9, and 0.4 MeV/nucleon respectively. The time evolutions of the density and the collective velocity are investigated. It is shown that the radial flow causes the system to expand in the isotropic direction, whereas the residual incident energy causes the system to extend along the longitudinal direction. Superposition of those two effects makes the system expand nonisotropically. It is supposed that the Pauli blocking is responsible for the residual incident energy and the nonisotropic nature of the collective velocity. The picture of self-similar expansion is shown along the longitudinal direction. However, the transverse expansion profile is non-self-similar but fits the relation between the collective velocity and radius of $\beta_r = \beta_0 r^\alpha$ with $\alpha > 1$.

ACKNOWLEDGMENTS

This work was supported by the National Natural Science Foundation of China under Grants No. 11025524 and No. 11161130520 and the National Basic Research Program of China under Grant No. 2010CB832903.

[1] C. Fuchs and H. H. Wolter, Eur. Phys. J. A **30**, 5 (2006).
[2] S. Wang *et al.*, Phys. Rev. Lett. **76**, 3911 (1996).
[3] B. Borderie, R. Bougault, P. Désesquelles, E. Galichet, B. Guiot, P. Lautesse, N. Le Neindre, J. Marie, M. Pârlog, M. Pichon, M. F. Rivet, E. Rosato, G. Tăbăcaru, M. Vigilante, and J. P. Wieleczko, Nucl. Phys. A **734**, 495 (2004).
[4] E. Bonnet *et al.* (INDRA and ALADIN Collaborations), Nucl. Phys. A **816**, 1 (2009).
[5] E. Bonnet *et al.*, Phys. Rev. Lett. **105**, 142701 (2010).
[6] N. Herrmann, J. P. Wessels, and T. Wienold, Annu. Rev. Nucl. Part. Sci. **49**, 632 (1997).
[7] W. Reisdorf and H. G. Ritter, Annu. Rev. Nucl. Part. Sci. **47**, 663 (1997).
[8] W. Bauer, Phys. Rev. C **51**, 803 (1995).
[9] P. J. Siemens and J. O. Rasmussen, Phys. Rev. Lett. **42**, 880 (1979).
[10] W. C. Hsi *et al.*, Phys. Rev. Lett. **73**, 3367 (1994).
[11] M. A. Lisa *et al.*, Phys. Rev. Lett. **75**, 2662 (1995).
[12] S. C. Jeong *et al.* (FOPI Collaboration), Phys. Rev. Lett. **72**, 3468 (1994).
[13] M. Petrovici *et al.* (FOPI Collaboration), Phys. Rev. Lett. **74**, 5001 (1995).
[14] G. Poggi *et al.* (FOPI Collaboration), Nucl. Phys. A **586**, 755 (1995).
[15] W. Reisdorf *et al.* (FOPI Collaboration), Nucl. Phys. A **612**, 493 (1997).

[16] J. C. Steckmeyer, Phys. Rev. Lett. **76**, 4895 (1996).
[17] R. Pak, D. Craig, E. E. Gualtieri, S. A. Hannuschke, R. A. Lacey, J. Lauret, W. J. Llope, N. T. B. Stone, A. M. Vander Molen, G. D. Westfall, and J. Yee, Phys. Rev. C **54**, 1681 (1996).
[18] S. C. Jeong *et al.*, Nucl. Phys. A **604**, 208 (1996).
[19] B. Borderie and M. F. Rivet, Prog. Part. Nucl. Phys. **61**, 551 (2008).
[20] G. D. Westfall, J. Gosset, P. J. Johansen, A. M. Poskanzer, W. G. Meyer, H. H. Gutbrod, A. Sandoval, and R. Stock, Phys. Rev. Lett. **37**, 1202 (1976).
[21] J. Gosset, J. I. Kapusta, and G. D. Westfall, Phys. Rev. C **18**, 844 (1978).
[22] L. P. Csernai and H. W. Barz, Z. Phys. A **296**, 173 (1980).
[23] J. P. Bondorf, S. I. A. Garpman, and J. Zimanyi, Nucl. Phys. A **296**, 320 (1978).
[24] G. J. Kunde *et al.*, Phys. Rev. Lett. **74**, 38 (1995).
[25] M. D'Agostino *et al.*, Phys. Lett. B **371**, 175 (1996).
[26] A. Le Fèvre *et al.*, Nucl. Phys. A **735**, 219 (2004).
[27] C. Hartnack and J. Aichelin, Phys. Lett. B **506**, 261 (2001).
[28] M. Colonna, G. Fabbri, M. Di Toroa, F. Matera, and H. H. Wolter, Nucl. Phys. A **742**, 337 (2004).
[29] L. W. Chen, F. S. Zhang, G. M. Jin, and Z. Y. Zhu, Phys. Lett. B **459**, 21 (1999).
[30] B. A. Bian, F. S. Zhang, and H. Y. Zhou, Chin. Phys. Lett. **24**, 1529 (2007).
[31] F. S. Zhang, B. A. Bian, and H. Y. Zhou, Int. J. Mod. Phys. E **17**, 1865 (2008).
[32] B. A. Li, G. C. Yong, and W. Zuo, Phys. Rev. C **71**, 044604 (2005).
[33] M. Colonna, V. Baran, M. Di Toro, and H. H. Wolter, Phys. Rev. C **78**, 064618 (2008).
[34] F. Gulminelli and P. Chomaz, Nucl. Phys. A **734**, 581 (2004).
[35] C. B. Das, L. Shi, and S. Das Gupta, Phys. Rev. C **70**, 064610 (2004).
[36] G. Stoicea *et al.*, Phys. Rev. Lett. **92**, 072303 (2004).
[37] J. Su and F. S. Zhang, Phys. Rev. C **87**, 017602 (2013).
[38] R. Wada *et al.*, Phys. Rev. C **62**, 034601 (2000).
[39] N. Marie *et al.*, Phys. Lett. B **391**, 15 (1997).
[40] W. Reisdorf *et al.* (FOPI Collaboration), Phys. Rev. Lett. **92**, 232301 (2004).
[41] F. Fu, Z. G. Xiao, Y. P. Zhang, Z. Q. Feng, G. M. Jin, H. S. Xua, N. Yao, X. H. Yuan, X. Y. Zhang, and M. Zhang, Phys. Lett. B **666**, 359 (2008).
[42] J. Aichelin, Phys. Rep. **202**, 233 (1991).
[43] C. Hartnack, L. Zhuxia, L. Neise, G. Peilert, A. Rosenhauer, H. Sorge, J. Aichelin, H. Stöcker, and W. Greiner, Nucl. Phys. A **495**, 303 (1989).
[44] R. J. Charity, M. A. McMahan, G. J. Wozniak, R. J. McDonald, L. G. Moretto, D. G. Sarantites, L. G. Sobotka, G. Guarino, A. Pantaleo, L. Fiore, A. Gobbi, and K. D. Hildenbrand, Nucl. Phys. A **483**, 371 (1988).
[45] J. Cugnon, D. L'Hôte, and J. Vandermeulen, Nucl. Instrum. Methods Phys. Res. B **111**, 215 (1996).
[46] G. D. Westfall *et al.*, Phys. Rev. Lett. **71**, 1986 (1993).
[47] M. Papa, T. Maruyama, and A. Bonasera, Phys. Rev. C **64**, 024612 (2001).
[48] F. S. Zhang, L. W. Chen, Z. Y. Ming, and Z. Y. Zhu, Phys. Rev. C **60**, 064604 (1999).
[49] J. Su, L. Zhu, W. J. Xie, and F. S. Zhang, Phys. Rev. C **85**, 017604 (2012).
[50] S. Hudan, Ph.D. thesis, Université de Caen, 2001 (unpublished).
[51] S. Hudan *et al.*, Phys. Rev. C **67**, 064613 (2003).